EAI Endorsed Transactions
on Energy Web
Research Article EAI.EU

Control Method for Overvoltage During Power Supply Loss in Medium-Voltage Flexible DC Sections Based on Guided Strategy Adaptive Particle Swarm Optimization

Asleng[1*], Jiadong Zhao[2], Peng Wang[2], Jun Guo[2], Ran Lu[1] and Yang Liu[2]

[1] Inner Mongolia Electric Power (Group) Co., Ltd.,Hohhot City, Inner Mongolia Autonomous Region, 010020, China
[2] Inner Mongolia Electric Power Group Mengdian Economic and Technological Research Institute Co., Ltd., Hohhot City, Inner Mongolia Autonomous Region, 010020, China

Abstract

To address the challenge of overvoltage control during power loss in medium-voltage flexible DC sections under complex and variable operating conditions, a control method based on guided-strategy adaptive particle swarm optimization (GS-APSO) is proposed to ensure voltage stability. This method analyzes the overvoltage formation mechanism during faults according to the topology of the medium-voltage flexible DC section. Building on this analysis, an adaptive nearest-level modulation (ANLM) strategy with voltage-limiting functionality is employed. The strategy adjusts the DC voltage based on the changes in the average submodule capacitor voltage, constraining the voltage near the target value. Furthermore, to enhance the overvoltage suppression performance, the guided-strategy adaptive particle swarm algorithm optimizes the voltage-limiting coefficient, deriving the coefficient that minimizes the overvoltage decay ratio, thereby improving the overvoltage loss control in the medium-voltage flexible DC section. The experimental results demonstrate that under different unbalanced power conditions, the proposed method achieves overvoltage control within 1.5 s, enabling rapid voltage recovery and stabilization. Even under significant power fluctuations, it effectively restricts the peak voltage variation range. After control, the overvoltage decay ratio remains below 0.015 on average.

Keywords: Guided Strategy; Adaptive Particle Swarm; Medium-Voltage Flexible; DC Section; Overvoltage Loss; ANLM Strategy

Received on 12 September 2025, accepted on 21 October 2025, published on 15 April 2026

doi: 10.4108/ew.12157

1. Introduction

Medium-voltage flexible DC transmission technology offers significant advantages, including flexibility, controllability, robust reactive power support, and multi-terminal interconnection capabilities. As a result, it is widely applied in distributed energy integration, urban grid expansion and renovation, and isolated island power supply systems. A medium-voltage flexible DC section refers to a transmission channel or connection zone constructed using medium-voltage flexible DC technology within a power system [1]. It can be regarded as a specific segment of the power transmission network, primarily relying on flexible DC technology to facilitate power transmission and exchange, thereby efficiently integrating distributed renewable energy sources into the medium-voltage distribution grid [2]. This helps mitigate the intermittency and volatility of renewable energy generation while improving the system's renewable energy accommodation capacity. However, medium-voltage flexible DC systems may experience sectional power-loss-induced overvoltage issues [3] during operation. When a section suddenly loses power due to faults, maintenance, or other disruptions, the energy balance within the system is compromised, leading to rapid capacitor energy discharge and a sharp rise in DC bus voltage, resulting in overvoltage. This overvoltage phenomenon not only inflicts severe damage on power electronic devices [4], reducing their operational lifespan, but may also trigger equipment failures, jeopardizing the safe and stable operation of the entire power grid. Therefore, in-depth research and effective mitigation of power-loss-induced overvoltage in medium-voltage flexible

* Corresponding author. Email: azmb2733005@163.com

DC systems are crucial for ensuring system reliability and enhancing grid stability [5]. Traditional control strategies primarily rely on hardware-based protection measures, such as surge arresters and capacitor-resistor absorption circuits. However, these approaches often struggle to achieve rapid and precise control under complex and variable operating conditions, and parameter tuning remains challenging, failing to meet modern power grids' demands for high reliability and flexibility [6].

Shanmugam et al. [7] establish a system model based on the operational characteristics of the power generation system and busbar to achieve voltage stability control. They employ feedback linearization to transform the nonlinear system into a linear one. For the resulting linear system, a linear controller is designed and then inversely transformed back to the original nonlinear system to derive the nonlinear control law. This serves as the foundation for nonlinear control of the grid-side converter, enabling the conversion of excess power caused by grid faults to achieve voltage stabilization. However, this method exhibits limited adaptability in practical applications. Specifically, under grid fault conditions, if the fault characteristics vary, the control strategy cannot promptly adapt to these changes, thereby compromising its effectiveness. Zhou et al. [8] propose a reactive power regulation strategy based on a static var compensator (SVC) to achieve effective voltage control and ensure stable operation. This strategy monitors the control bus voltage in real-time and incorporates multiple optimization metrics, including maximum voltage deviation, stabilization time, steady-state voltage deviation, and average voltage deviation during fluctuations. A genetic algorithm is utilized to optimize the controller parameters, thereby improving its response to voltage fluctuations. Nevertheless, the static var generator is constrained by the rotor current and stator voltage in the system. Under abrupt changes in operating conditions, the strategy fails to deliver sufficient reactive power support, resulting in delayed voltage regulation. Raza et al. [9] combine adaptive droop control with a voltage margin controller to ensure voltage stability. The voltage margin controller determines the stable DC voltage limit, while the droop coefficient manages the DC voltage. During significant power disturbances, power distribution is adjusted by switching the control modes of the rectifier and inverter, with regulation planned based on the DC voltage stability limit. However, if the system operates under fault conditions, the control strategy may exhibit insufficient response speed and adjustment capability, leading to imbalanced power distribution. Fagundes et al. [10] integrate charge balancing and droop control based on the system's operational structure to achieve effective voltage regulation. They define a normal operating range for the DC voltage. When the voltage exceeds the upper or lower limits, the power reference value is adjusted to modify the droop curve, thereby regulating the voltage and completing the system's secondary voltage recovery to ensure dynamic stability. However, under substantial charge variations, the balancing process may induce significant DC voltage fluctuations, diminishing the control effectiveness.

The guided-strategy adaptive particle swarm optimization (GS-APSO) algorithm is an enhanced version of the basic particle swarm optimization algorithm that incorporates both guidance strategies and adaptive mechanisms. The guidance strategy provides an effective search direction for the particle swarm optimization process, preventing the algorithm from converging to local optima while improving search efficiency [11]. The adaptive mechanism dynamically adjusts algorithm parameters according to the system's real-time operating conditions, ensuring robust performance across various operational scenarios. Based on this framework, this paper proposes a control method for power-loss-induced overvoltage in medium-voltage flexible DC systems using the GS-APSO algorithm. The method performs real-time optimization and adjustment of the flexible DC system's control parameters to achieve fast and precise overvoltage suppression during sectional power loss events. This approach is expected to effectively mitigate power-loss-induced overvoltage, enhance system stability and reliability, and provide substantial technical support for further development and application of medium-voltage flexible DC transmission technology.

2. Control of Overvoltage during Power Loss in Medium-Voltage Flexible DC Sections

2.1. Topological Structure of Medium-Voltage Flexible DC Section Operation

Medium-voltage flexible DC transmission represents an advanced power transmission approach based on voltage-source converters (VSCs), primarily employing modular multilevel converters (MMCs). MMCs utilize a staircase waveform approximation control principle, offering significant advantages including low power losses, minimal harmonic distortion, and excellent scalability, which have established them as the predominant technical solution for medium-voltage flexible DC transmission systems. The operational topological structure of a typical medium-voltage flexible DC section is illustrated in Figure 1.

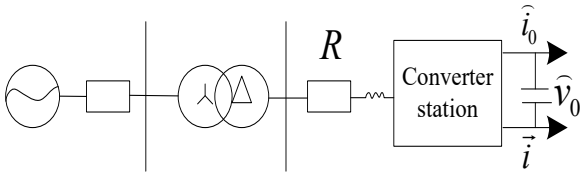

Fig. 1. Topological structure of medium voltage flexible DC section operation

Based on the operational topology of the medium-voltage flexible DC section shown in Figure 1, the mathematical

model of the converter's AC-side in the three-phase stationary coordinate system can be derived:

$$\begin{cases} L\dfrac{di_o^a}{dt} = v_o^a - Ri_o^a - v_e^a \\ L\dfrac{di_o^b}{dt} = v_o^b - Ri_o^b - v_e^b \\ L\dfrac{di_o^c}{dt} = v_o^c - Ri_o^c - v_e^c \end{cases} \tag{1}$$

Here, L denotes the equivalent inductance of the converter's AC-side; i_o^a, i_o^b and i_o^c represent the three-phase current; v_o^a, v_o^b and v_o^c represent the three-phase voltage; v_e^a, v_e^b and v_e^c represent the output voltage of the converter's AC-side; R represents the equivalent resistance of the converter's AC-side.

For a balanced three-phase grid, the mathematical model of the converter in the synchronous rotating reference frame can be expressed as:

$$\begin{cases} L\dfrac{di_o^d}{dt} = v_o^d + \omega L i_o^q - Ri_o^d - v_e^d \\ L\dfrac{di_o^q}{dt} = v_o^q + \omega L i_o^d - Ri_o^q - v_e^q \end{cases} \tag{2}$$

Where, v_o^d and v_o^q are the d and q component of the grid voltage; v_e^d and v_e^q are the d and q component of the converter's AC-side voltage; i_o^d and i_o^q are the d and q components of the AC current.

The DC-side dynamic equation can be expressed as:

$$C\frac{d\hat{v}_0}{dt} = \hat{i}_0 - \vec{i} \tag{3}$$

Where, C represents the DC-side capacitor; $\hat{v}_0$ indicates the converter's DC-side voltage; $\hat{i}_0$ represents the current flowing into the DC-side; $\vec{i}$ represents the load current on the DC-side.

The above formulation enables quantitative characterization of the converter's AC-side electrical characteristics. These equations facilitate analysis of the dynamic relationship between AC-side voltages and currents, as well as the effects of parameters such as inductance and resistance on system operation. This provides fundamental insights into the variation patterns of AC-side electrical quantities [12], establishing a theoretical foundation for subsequent power-loss overvoltage control strategies.

2.2. Mechanism of Power Outage Overvoltage

During a power outage in a medium-voltage flexible DC section, its active power output progressively decreases. Based on the operational topology and mathematical models analyzed previously, when such faults occur, the continuous active power collected at the sending-end converter station's AC side exceeds the receiving-end station's remaining power transmission capacity, leading to persistent accumulation of unbalanced energy within the flexible DC grid. Converter stations function as the grid's primary energy storage components, responsible for temporarily storing this unbalanced energy. The submodules (SMs), as core components of modular multilevel converters (MMCs), play a vital role in flexible DC transmission system performance. During AC faults in medium-voltage flexible DC sections, the energy storage variations in converter station arm inductors are negligible compared to those in receiving-end submodule capacitors. Thus, the station's energy storage can be effectively represented by the submodule capacitors' energy storage. When receiving-end AC faults occur, the combined action of capacitor voltage sequencing and voltage balancing algorithms causes alternating engagement/disengagement of submodules within each station, with sequential voltage increases [13], ultimately enabling unbalanced energy absorption. This energy accumulation raises the converter station's DC-side voltage, creating overvoltage conditions. Specifically, during fault conditions, the sending-end power source may continue injecting energy into the converter station while the receiving-end cannot promptly consume or transmit this energy due to the fault, causing DC-side energy accumulation that manifests as voltage elevation and overvoltage phenomena.

Let $t = 0$ denote the fault inception time. The expression for the capacitor voltage overvoltage transient in submodules within the flexible DC grid during the fault condition can be formulated as:

$$\begin{cases} \displaystyle\int_0^t \Delta P_\Sigma d\tau = 3N\sum_{i=1}^{m} C_i\left[v_c^2(t) - v_c^2(0)\right] \\ \Delta P_\Sigma = p_1 + p_2 + \ldots + p_i - \tilde{p}_0 \end{cases} \tag{4}$$

Where, ΔP_Σ is the system's excess power imbalance caused by the power outage of the entire section; N is the number of sub-modules; m is the number of converter stations involved in energy exchange; C_i is the capacitance value of the sub-modules in each converter station; v_c is the sub-module capacitor voltage at time t; $v_c(0)$ is the initial sub-module capacitor voltage at time $t = 0$; $p_i\,(i = 1, 2, \ldots, m)$ is the power on the DC side of each

converter station; $\tilde{p}_0$ indicates the network loss in the medium-voltage flexible DC section.

Since the regulation rate of the fixed DC voltage station is slower than the charging rate of the submodule capacitors, the unbalanced power ΔP can be considered constant during sectional power outages. Consequently, Equation (4) can be simplified as:

$$\Delta P \times t = 3N \sum_{i=1}^{m} C_i \left[v_c^2(t) - v_c^2(0) \right] \tag{5}$$

The DC voltage is supported by N series-connected submodules. Sectional power outages may induce overvoltage conditions, which can be analyzed through an equivalent capacitor model relating energy accumulation to voltage elevation. Consequently, the voltage rise dynamics due to unbalanced energy can be expressed as:

$$\begin{cases} \Delta P \times t = \dfrac{1}{2} C_\Sigma \left[\hat{v}_0^2(t) - \hat{v}_0^2(0) \right] \\ C_\Sigma = \dfrac{6}{N} \sum_{i=1}^{m} C_i \end{cases} \tag{6}$$

Where, C_Σ is the equivalent capacitance of the entire flexible DC grid; $\hat{v}_0^2(0)$ is the initial DC-side voltage of the converter at the time $t = 0$.

The aforementioned model quantitatively describes the static relationship between energy accumulation and voltage rise. However, in actual systems, the dynamic process of overvoltage depends not only on the initial power surplus but is also closely related to fault characteristics, control system response speed, and the coordination of control strategies across converter stations. For instance, the distinct energy release pathways and durations resulting from transient versus permanent faults significantly influence overvoltage peak levels and decay rates. Particularly in multi-terminal flexible DC systems, when a section loses power, the ability of neighboring healthy converter stations to rapidly provide power support or voltage reinforcement becomes critical for overvoltage suppression. Consequently, overvoltage mitigation is not merely a matter of local energy management but a dynamic process involving system-level coordination.

When the AC section of a flexible DC converter station loses power, the station loses its energy exchange channel with the AC system. The resulting DC overvoltage primarily stems from power surplus in the DC grid, which is intrinsically linked to the converter station's control mode and power transmission direction. The detailed mechanism can be analyzed as follows:

(1) For receiving-end stations employing fixed DC voltage control during sectional outages, the constant active power input from the sending end causes surplus power to accumulate in the submodule capacitors of both sending and receiving converters. This leads to continuous DC voltage $\hat{v}_0$ increase and severe DC-side overvoltage.

(2) In receiving-end stations with fixed active power control during outages, the DC voltage initially rises. If the fixed DC voltage station possesses sufficient regulation capacity (where surplus power remains within its regulation range), either reducing sending-end active power input or increasing receiving-end active power output to the AC grid [14] can maintain the DC voltage at its target value. This adjustment process duration depends critically on the fixed DC voltage station's control parameters.

(3) For sending-end stations with fixed DC voltage control during outages, the continued power absorption by receiving-end stations creates a DC system power deficit, causing continuous DC voltage $\hat{v}_0$ decrease without significant overvoltage.

(4) In sending-end stations with fixed active power control during outages, the fixed DC voltage station reduces its active power output to restore DC system power balance. Due to controller response time, the DC voltage experiences an initial drop before recovering to the target value, thereby avoiding sustained overvoltage conditions [15].

2.3. Overvoltage Control Strategy during Power Outages

Overvoltage Control Based on ANLM Strategy. Building upon the aforementioned analysis of power-loss-induced overvoltage mechanisms, this paper proposes an adaptive nearest-level modulation (ANLM) strategy incorporating voltage-limiting functionality to effectively mitigate power-loss overvoltage. The strategy dynamically adapts to precisely meet system voltage requirements, preventing both overvoltage and undervoltage conditions. Moreover, as key parameters of medium-voltage flexible DC systems - including submodule capacitance values and line impedance - may vary with operational conditions and environmental factors, the ANLM strategy autonomously adjusts its modulation approach based on these parametric variations to maintain reliable voltage limitation [16]. The strategy further demonstrates adaptive response capabilities for different fault scenarios: for AC-side fault-induced overvoltage, it reduces AC-to-DC energy injection through converter control parameter adjustment; for DC-side short-circuit faults, it enables rapid fault current interruption and overvoltage suppression.

The n-terminal converter station in the medium-voltage flexible DC grid adopts the ANLM strategy. Under these conditions, the equivalent capacitance of the flexible DC grid is calculated as follows:

$$C_\Sigma(t) = \left[\frac{1}{\eta^2} \frac{\sum_{i=1}^{m} C_i}{\sum_{i=1}^{n} C_i} + \frac{\sum_{i=n+1}^{m} C_i}{\sum_{i=1}^{n} C_i} \right] \frac{6}{N} \sum_{i=1}^{m} C_i \tag{7}$$

Where, $C_\Sigma(t)$ is the equivalent capacitance of the entire flexible DC grid at time t; η is the voltage limiting coefficient of the controller.

Consider a fault occurring at time $t=0$. At time $t=t_1$, the number of submodules begins to adaptively decrease to limit the DC voltage in the flexible DC grid. Subsequently, at time $t=t_2$, either the fault is cleared or the unbalanced power is removed, triggering a gradual recovery of submodule count. Finally, at time $t=t_3$, the number of submodules returns to its rated value. During the entire period from 0 to t_3, the DC voltage dynamics are governed by Equation (8):

$$\hat{v}_0(t)=\sqrt{\frac{2\Delta P\times t}{C_\Sigma(t)}+\frac{C_\Sigma(0)}{C_\Sigma(t)}\hat{v}_0^2(0)} \tag{8}$$

To maintain the DC voltage within the desired range $\varphi\hat{v}_0^2(0)$ during the period $t_1\sim t_3$, $C_\Sigma(t)$ must satisfy Equation (9):

$$C_\Sigma(t)=\frac{2\Delta P\times t+C_\Sigma(0)\hat{v}_0^2(0)}{\varphi\hat{v}_0^2(0)C_\Sigma(0)}C_\Sigma(0) \tag{9}$$

Where, φ is the ratio of the DC voltage target value to the steady-state value.

By combining equations (5) and (6), the formulas for calculating $C_\Sigma(t)$ and η can be derived as follows:

$$C_\Sigma(t)=\frac{v_c^2(0)}{\varphi^2\hat{v}_0^2(0)}C_\Sigma(0) \tag{10}$$

$$\eta=\sqrt{\frac{\varphi^2\chi_1}{\psi^2(t)-\varphi^2\chi_2}} \tag{11}$$

$$\psi(t)=\frac{\hat{v}_0(t)}{\hat{v}_0(0)}\sqrt{\frac{\chi_1}{\eta}+\chi_2} \tag{12}$$

Where $\chi_1=\dfrac{\sum_{i=1}^{n}C_i}{\sum_{i=n+1}^{m}C_i}$ and $\chi_2=\dfrac{\sum_{i=1}^{m}C_i}{\sum_{i=1}^{m}C_i}$.

If $m=n$, $\chi_1=1$ and $\chi_2=0$, then the calculation formulas for η and $\psi(t)$ are expressed as:

$$\eta=\frac{\varphi}{\psi(t)} \tag{13}$$

$$\psi(t)=\frac{\hat{v}_0(t)}{\eta N\hat{v}_0(0)} \tag{14}$$

As indicated in (15), when all converter stations in the medium-voltage flexible DC grid adopt the ANLM strategy, only the limiting voltage coefficient η must adapt to variations in the average capacitor voltage of the submodules within the medium-voltage flexible DC grid. This ensures that the DC voltage remains close to the reference value, thereby achieving overvoltage control during power interruptions in the grid.

Optimization of Limit Voltage Coefficient Based on Guided Strategy Adaptive Particle Swarm. The limiting voltage coefficient η in the ANLM strategy plays a critical role in overvoltage control performance. Under different operating conditions, topologies, and fault types of the medium-voltage flexible DC grid, the optimal limiting voltage coefficient may vary. To better accommodate the complex and dynamic operating states of the medium-voltage flexible DC grid and to ensure enhanced overvoltage control during power interruptions, this paper employs a guided adaptive particle swarm optimization algorithm to adjust the limiting voltage coefficient η. This improves the adaptability and robustness of the ANLM strategy, enabling it to maintain effective overvoltage control performance under various complex conditions.

To optimize the voltage limiting coefficient η, a well-designed objective function must be established to evaluate its performance, thoroughly considering both voltage recovery capability and system stability in the medium-voltage flexible DC grid following control actions. The voltage decay ratio during power loss is selected as the objective function. This ratio κ reflects the decay rate, directly indicating how quickly overvoltage decays within the system. A smaller decay ratio corresponds to faster overvoltage decay, leading to shorter recovery time to normal voltage levels; conversely, a larger ratio indicates slower decay, potentially requiring longer stabilization periods [17]. Furthermore, the voltage decay ratio serves as an indicator of system stability, implying that the medium-voltage flexible DC grid should rapidly attenuate overvoltage to safe levels following disturbances. An excessively large voltage decay ratio suggests weak voltage suppression capability, while a small ratio indicates effective suppression. Consequently, a minimization objective function for the voltage decay ratio is formulated, with its calculation expressed as follows:

$$\begin{cases}\min\kappa=\eta\dfrac{\bar{v}(t)}{\hat{v}_0(t)}\times100\%\\ s,t.\quad \eta_{\min}\le\eta\le\eta_{\max}\end{cases} \tag{15}$$

The voltage limiting coefficient η is determined using (15), with the undervoltage-overvoltage attenuation ratio optimized as the objective function. The guided adaptive particle swarm optimization algorithm is then employed to

enhance search capability. Under system constraints, the algorithm iteratively searches for the limiting voltage coefficient that minimizes the objective function. The algorithm improves particle updating by introducing four particle types during initial evolutionary stages [18]. These four particles form a hybrid system: primary particles, dual-center particles, cooperative particles, and chaotic particles. Their update strategy exchanges superior values obtained by dual-center, cooperative, and chaotic particles during each iteration with inferior components of primary particles. This approach adaptively guides particles toward optimal solutions, reduces algorithm randomness, and consequently improves search efficiency [19].

(1) Example of guiding strategy update optimization:

The guiding strategy update optimization is implemented through four distinct particle types introduced during the initial algorithm evolution phase:

(a) Primary particles serve as fundamental search units with randomly initialized positions covering the solution space, where each position represents a candidate solution for the undervoltage-overvoltage attenuation ratio optimization. Each primary particle's position corresponds to a set of limiting voltage coefficients η, which when substituted into the objective function yields the corresponding attenuation ratio for evaluating its proximity to the minimization requirement.

(b) Dual-center particles are derived from primary particles and exploit swarm centrality principles, where the optimal solution tends to emerge near the swarm's geometric center. These center particles accelerate algorithm convergence while maintaining standard particle properties including information sharing, position updating, and fitness evaluation. The dual-center approach leverages both individual and collective extremum positions, with the swarm center formed by particle extremums demonstrating higher probability of approaching optimal solutions. The dual-center particle calculation is expressed as follows:

$$x_1 = \frac{\sum_{i=1}^{n} x_i^z}{n} \tag{16}$$

$$x_2 = \frac{\sum_{i=1}^{n} \hat{x}_i^z}{n} \tag{17}$$

Where, x_1 represents the center of the main particles corresponding to a set of candidate limit voltage coefficients η; x_2 indicates the center of the individual extremum values representing a set of candidate limit voltage coefficients; x_i^z and $\hat{x}_i^z$ denote the position and the optimal position of the i-th limit voltage coefficient; z indicates the dimension.

(c) The third component comprises cooperative particles: implementing a cooperative mechanism, multiple independent particles representing candidate limiting voltage coefficient sets undergo single-dimensional updates along the global optimum position, while remaining coefficients η (particles) experience randomized z-dimensional updates to strengthen the algorithm's global exploration capability. The cooperative particle update formulation is expressed as:

$$x_i^z = \vec{x}_i^z + \gamma \times \Delta\upsilon \tag{18}$$

$$\Delta\upsilon = \upsilon_i^{\max}\left(1 - \beta\frac{\tau_o}{\tau_{\max}}\right) \tag{19}$$

Where, $\Delta\upsilon$ is the velocity variable during the update of the limited pressure coefficient η; τ_o is the current iteration number; $\tau_{\max}$ is the total number of iterations; β is the update coefficient; γ represents a random number.

(d) The fourth component involves chaotic particles: these particles are introduced through logistic mapping to generate near-boundary search particles (limiting voltage coefficients) within boundary-adjacent regions, addressing the algorithm's limitation in boundary-proximal exploration when particle initialization exhibits uneven distribution. The chaotic particle update formulation is expressed as:

$$\begin{cases} \lambda = 4\lambda(1-\lambda) \\ x_i^z = x_i^{\min} + t\left(x_i^{\max} - x_i^{\min}\right) \end{cases} \tag{20}$$

Where, $x_i^{\max}$ and $x_i^{\min}$ are the upper and lower bounds of x_i^z; λ is the chaotic factor.

(2) Gravitational measure strategy:

Following these adaptations, after completing the adaptive guidance for particles representing the limiting voltage coefficient η, the gravitational measure strategy optimizes the population structure and interaction processes within the hybrid particle swarm (comprising primary particles, center particles, cooperative particles, and chaotic particles). This strategy dynamically adjusts attraction-repulsion relationships between particles to enhance population diversity and convergence directionality. Based on Newton's law of universal gravitation, the strategy constructs inter-particle gravitational metrics to quantify interactions, enabling intelligent particle selection and guided population evolution. This methodology prevents algorithm stagnation in local optima caused by excessive particle clustering [20], while simultaneously amplifying the positive guidance of high-fitness particles through gravitational relationships. The approach effectively balances global exploration with local exploitation, refining particle interactions to significantly improve the algorithm's optimization performance.

If the gravitational measure is denoted as $g_{i,j}$, its calculation is expressed as:

$$g_{i,j} = \frac{f\left(x_i^z\right) * f\left(x_j^z\right)}{D_{i,j} + k} \tag{21}$$

Where, $f(.)$ is the fitness value of the limited pressure coefficient η to be optimized, $D_{i,j}$ is the Euclidean distance between the two limited pressure coefficients η in the two populations; k is a constant to ensure the denominator is not zero, and when k takes a larger value, the influence of $D_{i,j}$ on the gravitational measure can be ignored, thus avoiding very large gravitational measures when the distance is very small.

By utilizing the maximum individual-guided population evolution for $g_{i,j}$ obtained through the aforementioned process, the voltage limiting coefficient optimization is performed to determine the optimal limiting voltage coefficient η that minimizes both the voltage attenuation ratio during power loss and overvoltage conditions. The optimized coefficient η is then incorporated into Equation (14) to enhance the ANLM strategy's control performance. This enables effective adaptation to variations in the average capacitor voltage within medium-voltage flexible DC grid submodules, ensures reliable overvoltage control during power interruptions, facilitates restoration to the target voltage level, and maintains system stability.

3. Test Analysis

3.1. Test Object

To verify the effectiveness of the proposed control method for overvoltage mitigation in medium-voltage flexible DC systems during power outages, this paper conducts experimental validation based on a specific medium-voltage flexible DC grid project. The project integrates wind farms and photovoltaic power plants and consists of four converter stations, designated as Converter Stations 1 to 4. Among these, the sending-end converter stations are those connected to wind power and other power sources that transmit power outward, while the receiving-end converter stations are those connected to the AC main grid that absorb power. Specifically, the sending end comprises Converter Stations 1 and 3, which also function as rectifier stations. These stations are connected to wind power and other power sources via DC/AC converters and perform power transmission, thus classifying them as sending-end converter stations. The receiving end consists of Converter Stations 2 and 4, which also serve as inverter stations. These stations are directly or indirectly connected to the AC main grid and receive power, classifying them as receiving-end converter stations. They fulfill the role of power absorption and interconnection with the AC system. The topological structure of the project is illustrated in Figure 2, and the relevant parameters are provided in Table 1.

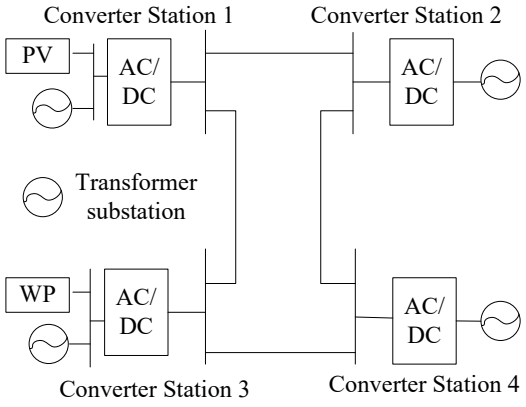

Fig.2. Topological structure of the voltage flexible DC power grid project

Table 1. Relevant parameters of medium voltage flexible DC power grid engineering

Parameter		Numerical value
DC line	Rated DC voltage	500kV
	Rated DC power	1000MW
	Resistance	50
	Inductance	1.2H
	Capacitance	26 μF
Delivery end (Converter Station 1 and Converter Station 3)	Conversion ratio of converter transformer	230/290.88kV
	Rated active power of converter station	1500MW, 3000MW
	Rated capacity of converter transformer	603.7 MVA
	Reactive power compensation capacity	626MVA
Receiver (Converter Station 2 and Converter Station 4)	Conversion ratio of converter transformer	525/290.88kV
	Rated active power of converter station	3000MW, 1500MW
	Reactive power compensation capacity	626MVA
	Rated capacity of converter transformer	591.8MVA

The system operating conditions during project execution are as follows: all stations operate at full power, with converter station 2 maintaining a fixed DC voltage. When a fault occurs on any receiving-end line or its subordinate lines, power imbalance may create a risk of power loss in the converter station 2 section, potentially leading to overvoltage during power loss events. This condition could compromise the overall stability and safety of the project. Therefore, to ensure the stability of the entire medium-voltage flexible DC grid, the method proposed in this paper is employed to control overvoltage during power loss conditions in the medium-voltage flexible DC section.

3.2. Analysis of Overvoltage Control Effect

When implementing the proposed control method for overvoltage mitigation during power loss in the medium-voltage flexible DC section, an adaptive nearest level modulation (ANLM) strategy with voltage limiting capability is developed, considering the structural and operational characteristics of this section. To evaluate the control performance of this method, overvoltage control at converter station 2 is conducted under different power imbalance conditions (200 kW and 400 kW) using the proposed approach, with the corresponding control results for this section presented in Figure 3.

As shown in Figure 3, Converter Station 2 encounters a power-loss overvoltage condition approximately 0.5 s after operation commencement, with the voltage rapidly exceeding 750 kV. By implementing the proposed power-loss overvoltage control method, Converter Station 2 successfully achieves voltage regulation within 1.5 s under both power imbalance conditions, enabling the voltage to quickly stabilize and maintain at 500 kV. The results demonstrate that this method can effectively adapt to different power imbalance conditions, successfully suppressing both the peak overvoltage and voltage fluctuations under various scenarios. This approach provides a reliable foundation for voltage safety control during power-loss conditions, ensuring system stability and safety under power-loss overvoltage situations.

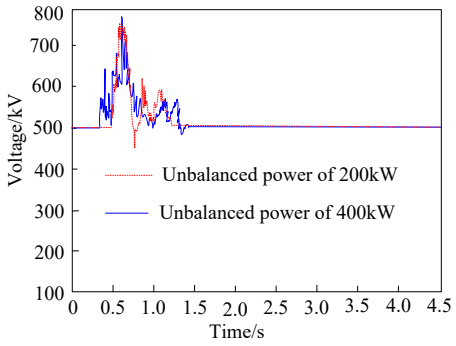

Fig. 3. Control results of overvoltage in converter station 2 during power loss

To further evaluate the application effectiveness of the proposed method, the voltage loss and overvoltage control approach is implemented under varying power fluctuation conditions in the medium-voltage flexible DC section. The peak values of both DC and AC voltages at the receiving end are measured before and after control implementation, with the results presented in Table 2.

Table 2. Results of peak changes in DC and AC voltage at the receiving end before and after control

Power fluctuation /%	Peak value of DC voltage /kV		AC voltage peak /kV	
	Before control	After control	Before control	After control
5	667	511	748	553
10	682	506	765	541
15	679	509	783	551
20	691	513	798	545
25	677	505	765	547
30	665	507	769	542
35	684	512	754	555
40	673	505	771	548
45	669	505	768	553
50	671	512	791	549

The test results in Table 2 demonstrate that the proposed method exhibits outstanding voltage peak suppression capability on both DC and AC sides as the power fluctuation amplitude increases from 5% to 50%. Prior to control implementation, the AC voltage peak shows a clear fluctuation trend correlated with increasing power fluctuation amplitude, varying from 748 kV to 798 kV. After control application, the AC voltage peak decreases substantially and stabilizes within the range of 541 kV to 555 kV. Notably, the method maintains effective voltage peak regulation despite significant variations in power fluctuation amplitude.

Furthermore, the DC voltage peaks also experience considerable reduction post-control. These results confirm that the proposed control method possesses strong adaptability and robustness, maintaining stable performance across different power fluctuation conditions while effectively preventing equipment damage from excessive voltage and ensuring safe operation of the medium-voltage flexible DC section.

3.3. Parameter Optimization Effect Analysis

For voltage loss and overvoltage control in the medium-voltage flexible DC section, the proposed method employs an adaptive particle swarm optimization algorithm with strategy-guided optimization of the voltage limit coefficient. To evaluate the optimization performance, the interval index ℓ_e is selected as a quantitative measure. The ℓ_e index quantifies the difference between adjacent solutions, with values ranging from 0 to 1 ($0 \le \ell_e \le 1$), where smaller values indicate a more uniform distribution of the solution set. The calculation formula for ℓ_e is as follows:

$$\ell_e = \sqrt{\frac{1}{M-1}\sum_{i=1}^{M}\left(\bar{d} - d_i\right)^2} \tag{22}$$

Where, d_i is the minimum Euclidean distance between the i-th non-dominated solution and other solutions; $\bar{d}$ is the average value of all d_i; M represents the number of potential solutions.

The proposed method is applied to optimize the voltage-limiting coefficient of the control strategy under both fault and transient operating conditions. As the number of potential solutions progressively increases, the resulting ℓ_e-index values obtained through the optimization process are presented in Table 3.

Table 3. Test results of interval indicators for parameter optimization

Potential solution quantity/piece	Operating conditions	
	Fault operation	Mutation operation
5	0.024	0.026
10	0.019	0.027
15	0.021	0.025
20	0.022	0.029
25	0.025	0.024
30	0.021	0.026
35	0.023	0.028
40	0.018	0.026
45	0.022	0.029
50	0.024	0.027

The test results in Table 3 demonstrate that when optimizing the voltage-limiting coefficient of the control strategy under different operating conditions using the proposed method, the ℓ_e-index values consistently maintain low levels despite the gradual increase in potential solutions. All optimized index values remain below 0.030, with the minimum ℓ_e-value reaching 0.018. These results confirm that the proposed method consistently identifies solutions with excellent distribution uniformity regardless of variations in the number of potential solutions. The method effectively balances solution diversity and convergence, providing a reliable foundation for control strategy development.

3.4. Comparative Method Analysis

To further validate the control performance of the proposed method, comparative experiments are conducted using the methods from references [6] and [8] as benchmarks. In the medium-voltage flexible DC grid test system, when load-side line faults occur, voltage sag overvoltage control is implemented under varying numbers of faulty lines. The voltage sag overvoltage attenuation ratio κ serves as the evaluation metric, with the comparative results of all three methods presented in Table 4.

Table 4 demonstrates that with increasing sending-end power and number of faulty lines in the medium-voltage flexible DC grid, the minimum voltage sag overvoltage attenuation ratios κ obtained using references [6] and [8] are 0.034 and 0.038 respectively, while the proposed method achieves a κ value below 0.015. The results show that under various sending-end power levels and fault line conditions, the proposed method reduces the voltage sag overvoltage attenuation ratio by an average of over 60% compared to the other methods, exhibiting superior overvoltage suppression performance. Furthermore, it provides more effective control of overvoltage attenuation for both single and multiple fault lines, demonstrating better adaptability to complex fault scenarios.

Table 4. Test results of voltage attenuation ratio after three control methods

Sending end power /kW	Number of faulty lines/line	Reference [6] method	Reference [8] method	Method in the text
100	1	0.036	0.041	0.014
	2	0.038	0.039	0.011
	3	0.034	0.044	0.013
300	1	0.035	0.043	0.011
	2	0.037	0.038	0.012
	3	0.034	0.042	0.009
500	1	0.036	0.041	0.013
	2	0.038	0.043	0.012
	3	0.035	0.038	0.015

While the single voltage decay ratio metric reflects control effectiveness, it is insufficient for comprehensively evaluating a method's practicality. Therefore, under stringent conditions of 500 kW feeder power and three faulty lines, the

voltage recovery time (defined as the time required for voltage to recover from peak to within 105% of rated value) and maximum overvoltage peak were selected as evaluation metrics. These were compared with the methods described in References [6] and [8], with results shown in Figure 4.

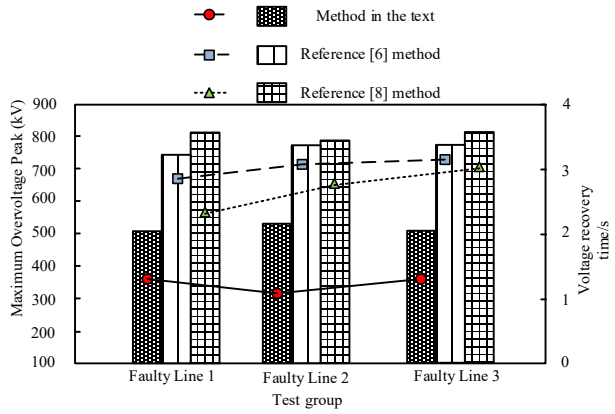

Fig. 4. Comparison of Practicality Among Three Methods Under Different Fault Conditions

As shown in Figure 4, the voltage recovery time of the proposed method is significantly shorter, consistently within 2 seconds. This indicates superior dynamic response capability, enabling rapid restoration of voltage to safe levels (within 105% of rated value) following a fault. This drastically reduces the duration of overvoltage exposure to equipment, allowing faster restoration of normal power supply capacity and thereby enhancing supply reliability and continuity. Moreover, the maximum overvoltage peak of this method is significantly lower than the two comparison methods, remaining around 500kV. This indicates that the proposed method can suppress voltage peaks below the insulation withstand level of equipment, effectively preventing breakdown damage due to transient overvoltage and reducing the risk of power outages caused by equipment failures. This is because the voltage-limiting coefficient optimized by the GS-APSO algorithm in this paper can adaptively adjust to the severity of the fault. This ensures that the ANLM strategy applies near-optimal voltage-limiting actions at the instant of the fault, accelerating energy rebalancing and voltage stabilization. Consequently, this method possesses high engineering application value.

4. Conclusion

This research presents an innovative control methodology employing a guided-strategy adaptive particle swarm optimization algorithm to address the critical challenge of power-loss overvoltage phenomena in medium-voltage flexible DC systems. Through comprehensive theoretical investigations, strategic framework development, and extensive experimental validations, three principal conclusions are established:

(1) A rigorous analysis of the power-loss overvoltage formation mechanism in medium-voltage flexible DC sections uncovers the fundamental relationship between submodule capacitor energy accumulation and subsequent DC voltage elevation. The developed Adaptive Nearest Level Modulation (ANLM) strategy demonstrates capability for dynamic voltage-limiting coefficient adjustment, achieving effective voltage fluctuation suppression while ensuring rapid DC voltage stabilization within the target operational range.

(2) The implemented guided-strategy adaptive particle swarm optimization algorithm, incorporating hybrid particle collaboration (including main particles, double-center particles, cooperative particles, and chaotic particles) complemented by gravitational measurement strategies, exhibits substantial enhancement in global optimization capability and convergence characteristics. The optimized voltage-limiting coefficients yield overvoltage attenuation ratios consistently below 0.015, representing a performance improvement exceeding 60% compared to conventional approaches.

(3) Experimental evaluations across diverse operational scenarios, including power imbalance conditions (200 kW-400 kW) and power fluctuation ranges (5%-50%), confirm the method's capability for rapid voltage stabilization with significant attenuation of both DC and AC voltage peak fluctuations. Furthermore, the methodology maintains consistent control performance under increasing fault line quantities, demonstrating exceptional robustness and operational adaptability in complex system conditions.

The proposed methodology fundamentally transcends the constraints inherent in conventional hardware protection schemes and singular control approaches by establishing a comprehensive "topology-energy-control" integrated overvoltage suppression framework. This innovative mechanism delivers robust technical foundations for ensuring operational safety in medium-voltage flexible DC transmission infrastructures while simultaneously contributing substantial value to renewable energy integration and power grid stability enhancement. Subsequent investigations should focus on developing advanced multi-objective cooperative optimization paradigms capable of addressing the increasingly complex operational requirements of modern multi-terminal DC grid architectures.

References

[1] Basati, S., Moradi, H., & Karimi, S. (2024). Voltage profile improvement in islanded DC microgrid using load shedding method based on DC bus voltage estimation. Electrical Engineering, 106(4), 4115-4125.

[2] Izci D, Rizk-Allah R M, Snášel V, et al. (2024). Refined sinh cosh optimizer tuned controller design for enhanced stability of automatic voltage regulation. Electrical engineering, 106(5):6003-6016.

[3] Heidary, J., Gheisarnejad, M., & Khooban, M. H. (2023). Stability Enhancement and Energy Management of AC-DC Microgrid based on Active Disturbance Rejection Control. Electric Power Systems Research, 217(Apr.):109105.1-109105.13.

[4] Jain, D., & Saxena, D. (2023). Comprehensive review on control schemes and stability investigation of hybrid AC-DC microgrid. Electric Power Systems Research, 218(May):1.1-1.18.
[5] Sagar, C., & Kumar, A. (2024). Investigations of Large-Scale Voltage-Dependent Loads for Damping Low-Frequency Oscillations: Decentralized Control. IEEE systems journal, 18(1):234-243.
[6] Ungerland, J., Poshiya, N., & Lens, B. H. (2023). A Voltage Sensitivity Based Equivalent for Active Distribution Networks Containing Grid Forming Converters. IEEE transactions on smart grid, 14(4):2825-2836.
[7] Shanmugam R, Sakthivel D K, Ramaiah A N, et al. (2024). Nonlinear Control Strategy for DC-Link Voltage Control in a DFIG of WECS During 3φ Grid Faults. IEEE Transactions on Industrial Electronics, 71(10 Pt.1):12468-12475.
[8] Zhou, Z., Mastoi, M. S., & Wang, D. H. M. (2023). Control strategy of DFIG and SVG cooperating to regulate grid voltage of wind power integration point. Electric Power Systems Research, 214(Jan. Pt.A):1-13.
[9] Raza, A., Huang, Q., Li, J., Bamisile, O., et al. (2024). A coordinated control scheme for VSC-MTDC system with multiple renewable energy sites based on voltage margin and adaptive drooping control. International Journal of Control, 97(7/9):1658-1674.
[10] Fagundes, T. A., Fuzato, G. H. F. , Magossi, R. F. Q., et al. (2024). Secondary Voltage Control for DC Microgrids: A Design Perspective for SoC With Voltage Restoration Provision. IEEE transactions on smart grid, 15(6):5773-5786.
[11] Sun, P., Konstantinou, G., & Wang, Y. K. M. B. R. (2023). Steady-state power distribution in VSC-based MTDC systems and dc grids under mixed P/V and I/V droop control. Electric Power Systems Research, 214(Jan. Pt.A):1-10.
[12] Pacheco-Cherrez, D. S., Guillen, D., Mayo-Maldonado, J. C., et al. (2024). Data-Driven Optimal Voltage Performance Index Tracking in Active Distribution Networks. IEEE transactions on smart grid, 15(5):4804-4818.
[13] Gorjian, A., Eskandari, M., & Moradi, M. H. (2024). Multi-agent deep reinforcement learning for joint dynamic conservation voltage reduction and Q-sharing in inverter-based autonomous microgrids. Electric Power Systems Research, 231(Jun.):1.1-1.12.
[14] Nasir, M., Sadollah, A., Barati, H., et al. (2024). Generation Rescheduling Based Contingency Constrained Optimal Power Flow Considering Uncertainties Through Stochastic Modeling. IETE journal of research, 70(5):4917-4939.
[15] Kakroudi, S. A., Ebrahimi, R., & Ahmadi, A. (2023). Real-time under-voltage load shedding method considering integer-value load model and feeder participation in demand response. Electric Power Systems Research, 217(Apr.):109115.1-109115.12.
[16] Ibraheem, M. I., Edrisi, M., Alhelou, H. H., et al. (2024). Fractional order slide mode droop control for simultaneous voltage and frequency regulation of AC microgrid. IET renewable power generation, 18(14):2629-2640.
[17] Zhang,Y. B., Zou, D.X., Zhang, C.,Y.,et al. (2023). Particle Swarm Optimization Algorithm with Adaptive Inertial Weight. Computer Simulation,40(4):350-357.
[18] Soliman, A. S., Rafin, S. M. S. H., & Mohammad, O. A. (2024). Enhanced DC Voltage and Power Regulation Using Intelligent Data-Driven Control for AC/DC Converters in DC Microgrid Applications. IEEE Transactions on Industry Applications, 60(6 Pt.1):8383-8392.
[19] Vensila, C., & Wesley, A. B. (2024). Multimodal biometrics authentication using extreme learning machine with feature reduction by adaptive particle swarm optimization. The visual computer, 40(3):1383-1394.
[20] Sawant, S. S., Erick, F. X., Goeb, S., et al. (2023). An adaptive binary particle swarm optimization for solving multi-objective convolutional filter pruning problem. Journal of supercomputing, 79(12):13287-13306.